Ferroelectric Valence Transition and Phase Diagram of a Series of Charge-Transfer Complexes of 4,4′-Dimethyltetrathiafulvalene and Tetrahalo-*p*-benzoquinones

Sachio Horiuchi,*,† Yoichi Okimoto,† Reiji Kumai,† and Yoshinori Tokura†,‡

Contribution from the Joint Research Center for Atom Technology (JRCAT), Tsukuba 305-0046, Japan, and Department of Applied Physics, The University of Tokyo, Tokyo 113-8656, Japan

Received May 15, 2000. Revised Manuscript Received September 6, 2000

Abstract: Variation of the ferroelectric phase transition has been investigated for a series of isomorphous donor (*D*)−acceptor (*A*) charge-transfer complexes composed of 4,4′-dimethyltetrathiafulvalene (DMTTF) and tetrahalo-*p*-benzoquinones by measurements of dielectric susceptibility, X-ray diffraction, and infrared molecular vibrational spectra. The neutral−ionic phase transition of DMTTF−*p*-chloranil at 65 K accompanies a dielectric peak anomaly associated with the *DA* stack dimerization. Successive halogen replacement by bromine in the component tetrahalo-*p*-benzoquinone molecule expands the lattice along the *DA* stack of the DMTTF complex, and reduces the critical temperature steeply toward zero temperature in an analogous way to the critical behavior of quantum ferroelectrics. The 2,6-dibromo-substituted compound showing the behavior of the quantum paraelectricity is located in the immediate vicinity of the quantum critical point of this phase diagram as signified also by enhancement of the ionicity, the dielectric susceptibility, and the dynamical dimeric distortion at the lowest temperature.

Introduction

The ground state of organic charge-transfer (CT) complexes having alternately stacked electron donor (*D*) and acceptor (*A*) molecules may traverse the neutral−ionic (NI) boundary, when the delicate balance is altered between the effective ionization energy of a *D*−*A* pair and the long-range electrostatic energy gain.[1] Although only a very few among a handful CT complexes have been found to thermally experience such an unusual valence transition called the NI transition at ambient pressure,[2−4] their optical, magnetic, dielectric, and conducting properties have been attracting considerable interest.[5−7] In particular, upon the transformation to the ionic state, the *DA* stack carrying $S = {}^1/_2$ spins in the constituent molecules shows a spin-Peierls-like dimeric distortion as can be schematized as follows: $D^0\,A^0\,D^0\,A^0\,D^0\,A^0\,D^0\,A^0 \rightarrow \underline{D^+A^-}\;\underline{D^+A^-}\;\underline{D^+A^-}\;\underline{D^+A^-}$.

This appears as a special class of ferroelectric phase transition, since the stack of dimerized D^+A^- pairs shown by the underlines above carries an electric dipole.[8]

Recently, to control this novel phase transition and related properties, a variety of materials have been explored by the chemical modification of *D* and *A* molecules. The studies of alloyed crystals based on the prototype compound tetrathiafulvalene (TTF)−*p*-chloranil (QCl_4) have led us to some interesting dielectric phenomena depending on the nature of the dopant molecules: quantum ferro-/para-electricity in the nominally negative pressure region ("chemical pressure" effect) and the diffuse phase transition or the so-called "relaxor" behavior due to the microscopic binary phase separation.[9] An alternative approach focuses on a successive replacement of the substituents in molecules to minimize the inhomogeneity effect which is inevitable for the alloyed molecular system. Changing one Cl substituent by a Br in TTF−QCl_4, rapid valence fluctuation between the neutral and ionic states becomes visible near the diminished critical temperature (T_c).[10] In the present work with use of *D* = 4,4′-dimethyltetrathiafulvalene (DMTTF), we demonstrate the fine-tuning of the ground state using "chemical pressure" by varying the number of Br substituents (*n*) systematically from 0 to 4 in tetrahalo-*p*-benzoquinones (rep-

† Joint Research Center for Atom Technology.

‡ The University of Tokyo.

(1) (a) McConnell, H. M.; Hoffman, B. M.; Metzger, R. M. *Proc. Natl. Acad. Sci. U.S.A.* **1965**, *53*, 46. (b) Soos, Z. G.; Mazumdar, S. *Phys. Rev.* **1978**, *B18*, 1991. (c) Torrance, J. B.; Vazquez, J. E.; Mayerle, J. J.; Lee, V. Y.; *Phys. Rev. Lett.* **1981**, *46*, 253.

(2) Torrance, J. B.; Girlando, A.; Mayerle, J. J.; Crowley, J. I.; Lee, V. Y.; Batail, P.; LaPlaca, S. J.; *Phys. Rev. Lett.* **1981**, *47*, 1747.

(3) (a) Iwasa, Y.; Koda, T.; Tokura, Y.; Kobayashi, A.; Iwasawa, N.; Saito, G. *Phys. Rev.* **1990**, *B42*, 2374. (b) Aoki, S.; Nakayama, T. *Phys. Rev.* **1997**, *B56*, 2893.

(4) (a) Aoki, S.; Nakayama, T.; Miura, A. *Phys. Rev.* **1993**, *B48*, 626. (b) Aoki, S.; Nakayama, T.; Miura, A. *Synth. Met.* **1995**, *70*, 1243.

(5) (a) Tokura, Y.; Koda, T.; Mitani, T.; Saito, G. *Solid State Commun.* **1982**, *43*, 757. (b) Koshihara, S.; Takahashi, Y.; Sakai, H.; Tokura, Y.; Luty, T. *J. Phys. Chem. B* **1999**, *103*, 2592. (c) Mitani, T.; Saito, G.; Tokura, Y.; Koda, T. *Phys. Rev. Lett.* **1984**, *53*, 842. (d) Okamoto, H.; Mitani, T.; Tokura, Y.; Koshihara, S.; Komatsu, T.; Iwasa, Y.; Koda, T.; Saito, G. *Phys. Rev.* **1991**, *B43*, 8224. (e) Tokura, Y.; Okamoto, H.; Koda, T.; Mitani, T.; Saito, G. *Phys. Rev.* **1988**, *B38*, 2215. (f) Lemée-Cailleau, M. H.; Le Cointe, M.; Cailleau, H.; Luty, T.; Moussa, F.; Roos, J.; Brinkmann, D.; Toudic, B.; Ayache, C.; Karl, N. *Phys. Rev. Lett.* **1997**, *79*, 1690.

(6) Girlando, A.; Marzola, F.; Pecile, C.; Torrance, J. B. *J. Chem. Phys.* **1983**, *79*, 1075.

(7) (a) Hubbard, J.; Torrance, J. B. *Phys. Rev. Lett.* **1981**, *47*, 1750. (b) Nagaosa, N. *J. Phys. Soc. Jpn.* **1986**, *55*, 2754 and 3488. (c) Cailleau, H.; Lemée-Cailleau, M. H.; Le Cointe, M.; Luty, T. *Acta Phys. Pol.* **1997**, *A92*, 597.

(8) Le Cointe, M.; Lemée-Cailleau, M. H.; Cailleau, H.; Toudic, B.; Toupet, L.; Heger, G.; Moussa, F.; Schweiss, P.; Kraft, K. H.; Karl, N. *Phys. Rev.* **1995**, *B51*, 3374.

(9) (a) Horiuchi, S.; Kumai, R.; Tokura, Y. *J. Am. Chem. Soc.* **1998**, *120*, 7379. (b) Horiuchi, S.; Kumai, R.; Okimoto, Y.; Tokura, Y. *Phys. Rev.* **1999**, *B59*, 11267.

(10) Horiuchi, S.; Okimoto, Y.; Kumai, R.; Tokura, Y. *J. Phys. Soc. Jpn.* **2000**, *69*, 1302.

10.1021/ja0016654 CCC: $20.00
Published on Web 01/05/2001

Table 1. Crystal Data and Experimental Details for DMTTF−QBr_nCl_{4-n} Complexes (chemical formula $C_{14}H_8O_2S_4Cl_{4-n}Br_n$)

Br content n in QBr_nCl_{4-n}	0	1	2 (2,5)	2 (2,6)	3	4
formula wt	478.27	522.72	567.17	567.17	611.62	656.07
a/Å	7.678(1)	7.707(2)	7.717(3)	7.733(3)	7.754(2)	7.775(2)
b/Å	8.521(1)	8.660(2)	8.778(3)	8.754(3)	8.873(2)	8.951(1)
c/Å	7.285(4)	7.321(2)	7.338(4)	7.353(5)	7.382(4)	7.416(2)
α/deg	103.89(2)	104.94(2)	105.98(3)	105.70(4)	106.59(3)	107.11(1)
β/deg	91.91(2)	91.84(2)	91.75(4)	91.67(4)	91.58(3)	91.56(2)
γ/deg	95.90(1)	95.91(2)	95.91(3)	95.80(3)	95.91(2)	96.02(2)
V/Å^3	459.4(3)	468.8(2)	474.4(4)	475.9(4)	483.3(3)4	89.6(2)
space group	$P\bar{1}$	$P\bar{1}$	$P\bar{1}$	$P\bar{1}$	$P\bar{1}$	$P\bar{1}$
ρ_{calc}/g cm^{-3}	1.73	1.85	1.99	1.98	2.10	2.22
Z	1	1	1	1	1	1
dimensions/mm	0.45 × 0.20 × 0.15	0.30 × 0.27 × 0.06	0.28 × 0.15 × 0.10	0.25 × 0.16 × 0.15	0.50 × 0.19 × 0.08	0.50 × 0.14 × 0.04
$2\theta_{max}$/deg	55	55	55	55	55	55
scan technique	2θ-ω	2θ-ω	2θ-ω	2θ-ω	2θ-ω	2θ-ω
scan speed/deg(ω)	16	16	16	16	16	16
total reflcn	2098	2151	2168	2178	2221	2257
reflcn used ($6\sigma(I) < I$)	1752	1656	1582	1659	1836	1533
no. of variables	109	110	110	109	110	109
R	0.026	0.048	0.042	0.029	0.031	0.038
R_w	0.029	0.057	0.048	0.029	0.034	0.036
weighting scheme	$1/\sigma^2$	$1/\sigma^2$	$1/\sigma^2$	$1/\sigma^2$	$1/\sigma^2$	$1/\sigma^2$
GOF	2.09	2.83	1.85	1.09	1.83	2.47

resented as QBr_nCl_{4-n}, see below) with little perturbation on

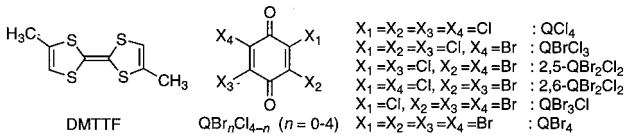

their electron affinity.[11] (Note that the TTF−QBr_nCl_{4-n} has no isomorphous crystals for $n \geq 2$.[10,12]) The parent system DMTTF−QCl_4 is the recently discovered compound undergoing the thermally induced NI transition.[4] On the basis of dielectric, structural, and optical properties, we report the whole phase diagram of the valence state and the related ferro-/paraelectricity, which can be drawn across the quantum critical point ($T = 0$ K transition point) for the first time on the nonalloy system.

Experimental Section

Purchased DMTTF, QCl_4, and QBr_4 and the other QBr_nCl_{4-n} which were synthesized by bromination of the corresponding chlorinated quinones[13] were purified by repeated recrystallization and vacuum sublimation processes. Concomitants of $n \pm 1$ homologues in the QBr_nCl_{4-n} ($n = 1-3$) detected by mass spectroscopy were eliminated by supercritical fluid chromatography eluting with CO_2.[10] Single crystals of DMTTF−QBr_nCl_{4-n} ($n = 0-4$) complexes were grown by cosublimation of the purified component materials in a vacuum-sealed Pyrex glass tube, which is placed at the temperature of 70−110 °C in an electric furnace for several days.

The crystal structures of DMTTF complexes at room temperature were determined with use of a Rigaku AFC7R four-circle diffractometer and graphite-monochromated Mo Kα radiation. All the calculations were made on the teXsan crystallographic software package of the Molecular Structure Corporation. The hydrogen atoms were not included in the least-squares refinements. The QBr_nCl_{4-n} ($n = 1-3$) molecules show the orientational disorder with respect to two crystallographically independent Cl/Br sites, the occupation of which were determined by population analysis except for the 2,6-QBr_2Cl_2 with equal Br/Cl ratios. The final refinements of non-hydrogen atoms were done with anisotropic thermal factors. The crystal data and experimental details are summarized in Table 1.

The dielectric constant was measured with an LCR meter (HP 4284A) using a four-probe configuration. The ac electric field was applied parallel to the *DA* stack on to the crystal end sections, which were painted with gold paste as electrodes. Polarized infrared reflection spectra on a single crystal were collected with 2 cm^{-1} resolution with use of an FT-IR spectrometer (Nicoley, Magna560) equipped with a microscope and an MCT (HgCdTe) detector.

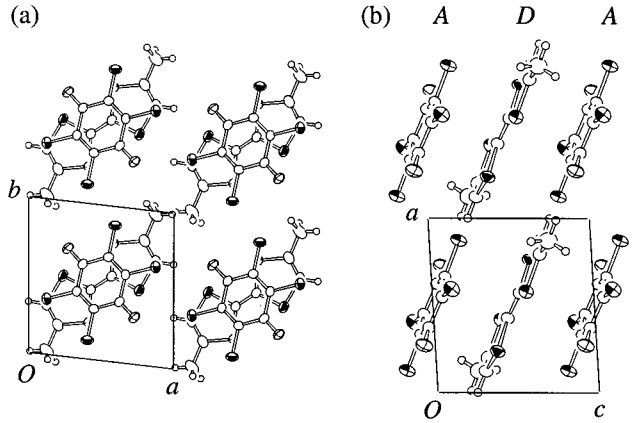

Figure 1. Crystal structure of DMTTF−QBr_nCl_{4-n} at room temperature (space group, $P\bar{1}$) showing the mixed stack of donor (*D*) and acceptor (*A*) molecules viewed along the *c* (*DA* stacking) direction (a) and the *b* direction (b).

Results and Discussion

Structural Properties of DMTTF−QBr_nCl_{4-n}. Figure 1 shows the crystal structures of DMTTF−QBr_nCl_{4-n} complexes at room temperature. They are centrosymmetric with triclinic ($P\bar{1}$) isostructure, which is comprised of the uniform *DA* mixed stack along the *c* direction. The QBr_nCl_{4-n} molecules of $n = 1-3$ lying on the center of inversion show an orientational disorder with respect to the two crystallographically independent halogen sites. The analysis gave the different Br/Cl population ratios on the two inequivalent sites, except for the 2,6-QBr_2Cl_2 having the inevitably equal probability (Br/Cl = 1). The lattice parameters plotted as a function of Br content n in Figure 2

(11) Chen, E. C. M.; Wentworth, W. E. *Mol. Cryst. Liq. Cryst.* **1989**, *171*, 271.
(12) Sadohara, R.; Matsuzaki, S. *Mol. Cryst. Liq. Cryst.* **1997**, *296*, 269.
(13) Ling, A. R. *J. Chem. Soc.* **1892**, *61*, 558.

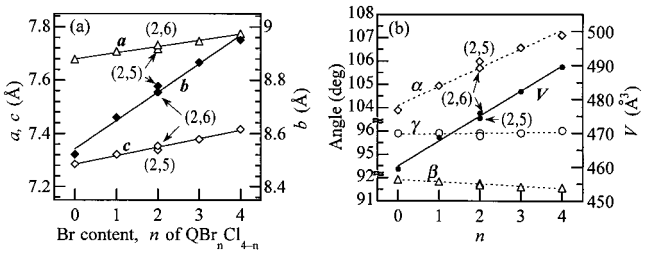

Figure 2. Lattice parameters of DMTTF−QBr_nCl_{4-n} crystals (tricilinic, $P\bar{1}$) with various numbers (n) of Br substituents: (a) cell lengths a (open triangles), b (filled squares), and c (open squares) and (b) cell angles α (open squares), β (open triangles), and γ (open circles) and volume V (filled circles).

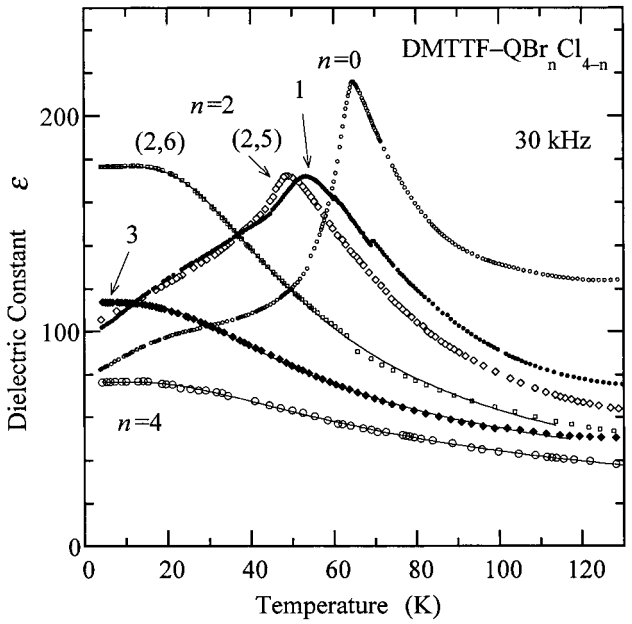

Figure 3. Temperature dependence of the dielectric constant (ϵ) measured at 30 kHz for DMTTF−QBr_nCl_{4-n} complexes. Solid curves for $n = 2$ (2,6), 3, and 4 represent the fit to the Barrett formula (eq 1) describing the quantum paraelectricity.

depict the appreciable lattice expansion with increasing size of the quinones. The 2,6-substitution resulted in looser molecular packing (cell volume, $V = 475.9$ Å^3) than the symmetric 2,5-QBr_2Cl_2 isomer (474.5 Å^3), giving rise to the distinct properties as shown below.

Dielectric Properties. Three-dimensional arrangement of polar *DA* dimers in the low-temperature phase of the DMTTF−QCl_4 crystal has been deduced to be a ferroelectric-type (noncentrosymmetric space group, $P1$) by the X-ray diffraction measurements,[14] although no study has so far been made on the dielectric properties. Figure 3 shows the dielectric constant (ϵ) measured along the *DA* stacking axis for a series of DMTTF complexes. The $\epsilon-T$ curve of DMTTF−QCl_4 displays a sharp anomaly characteristic of a ferroelectric transition at 65 K that agrees with the critical temperature (T_c) for the NI transition deduced from the optical measurements. Similar $\epsilon-T$ curves are found for the complexes of $QBrCl_3$ and 2,5-QBr_2Cl_2 with reduced T_c. On the other hand, the peak anomaly is smeared out for the complex of the other $n = 2$ isomer 2,6-QBr_2Cl_2 having a slightly larger V: ϵ increases to about 180 in cooling but becomes nearly temperature independent below 15 K. This $\epsilon-T$ curve can be well fitted to the Barrett formula[15] describing the quantum fluctuation effect on ϵ so as to deviate from the Curie−Weiss law:

$$\epsilon = A + B/[(T_1/2)\coth(T_1/2T) - T_0] \quad (1)$$

Here, the parameter T_0 equals the Curie−Weiss temperature in a classical (high T) limit, and T_1 represents the characteristic crossover temperature dividing the quantum mechanical and classical region. The best fitting of the data, which is drawn by solid curves in Figure 3, gives $T_0 = 28 \pm 1$ K and $T_1 = 108 \pm 1$ K for the 2,6-QBr_2Cl_2 complex. In light of the Curie−Weiss behavior, the ferroelectric transition is expected near this positive T_0. Nevertheless, the complete absence of phase transition indicates the importance of quantum fluctuation, namely the quantum paraelectricity.[15] The complexes of QBr_3Cl and QBr_4 remain paraelectric over the entire temperature range: the T_0 (2 and −32 K, respectively) and the low-temperature susceptibility are further diminished with increasing n, indicating the ground state gradually released from the ferroelectric lattice instability.

Ionicity ρ. For the tetrahalo-*p*-benzoquinone complexes, the degree of CT (ρ) can be estimated by the frequency shift of the infrared-active C═O stretch mode, which shows a very large ionization shift (−160 cm^{-1} upon complete ionization).[16] This vibrational band can be observed in the infrared spectra with the electric vector (E) perpendicular to the *DA* stacking direction of a single crystal.

Figure 4 shows the thermal behavior of this vibrational band in the optical conductivity spectra, which were deduced from the polarized reflectivity spectra by Kramers−Kronig transformation. The C═O stretch mode of DMTTF−QBr_nCl_{4-n} displays a single band except for the 2,6-QBr_2Cl_2 complex showing doublet bands (Figure 4c). The mode splitting of about 10 cm^{-1} for the 2,6-QBr_2Cl_2 complex, as is evident in the spectra of $\rho = 0$ species, is ascribable to the inequivalence of the two C═O groups in the asymmetric molecule rather than to an inhomogeneous ρ in the crystal.[17] The phase transition of a DMTTF−QCl_4 crystal at $T_c = 65$ K manifests itself as a conspicuous shift of this vibrational band (Figure 4a) due to the ionicity change. The increment of Br content in QBr_nCl_{4-n} appears to diminish the thermal change of the ρ-sensitive C═O band spectra of the DMTTF complexes.

Figure 5a depicts the temperature-dependent ρ for the DMTTF complexes, which was deduced by assuming the linear relation between ρ and the frequency shift as

$$\rho = (\omega_{C=O} - \omega_{C=O}{}^{(0)})/\Delta\omega_{C=O} \quad (2)$$

Here, $\omega_{C=O}$ is the C═O stretching frequency, $\omega_{C=O}{}^{(0)}$ the frequency at $\rho = 0$, and $\Delta\omega_{C=O}$ the frequency shift upon complete ionization of the quinones.[18] For the 2,6-QBr_2Cl_2 complex, the weight-averaged $\omega_{C=O}$ values of the split bands are used to calculate ρ values in Figure 5a. All the DMTTF

(14) Nogami, Y.; Taoda, M.; Oshima, K.; Aoki, S.; Nakayama, T.; Miura, A. *Synth. Met.* **1995**, *70*, 1219.

(15) (a) Müller, K. A.; Burkard, H. *Phys. Rev.* **1979**, *B19*, 3593. (b) Barrett, J. H. *Phys. Rev.* **1952**, *86*, 118.

(16) Girlando, A.; Zanon, I.; Bozio, R.; Pecile, C. *J. Chem. Phys.* **1978**, *68*, 22.

(17) The C═O stretching mode of the neutral QBr_nCl_{4-n} solid (in KBr) shows a doublet with splitting of ca. 10 cm^{-1} due to the asymmetric crystal field at the two C═O groups.[16] Further mode splitting is visible only for the 2,6-QBr_2Cl_2 (peaks at 1690, 1682, 1675 cm^{-1}), which, among the QBr_nCl_{4-n} molecules, has the most conspicuous inequivalency in the force field on the two C═O groups due to the asymmetric weight of the adjacent C−Cl/Br groups.

(18) $\omega_{C=O}{}^{(0)}$ and $\Delta\omega_{C=O}$: QCl_4, 1685, −162 cm^{-1}; 2,5-QBr_2Cl_2, 1681, −165 cm^{-1}; 2,6-QBr_2Cl_2, 1682, −168 cm^{-1}; QBr_3Cl, 1679, −167 cm^{-1}; QBr_4, 1676, −169 cm^{-1}. Potassium salts of QBr_nCl_{4-n} were used for the $\rho = 1$ standard.

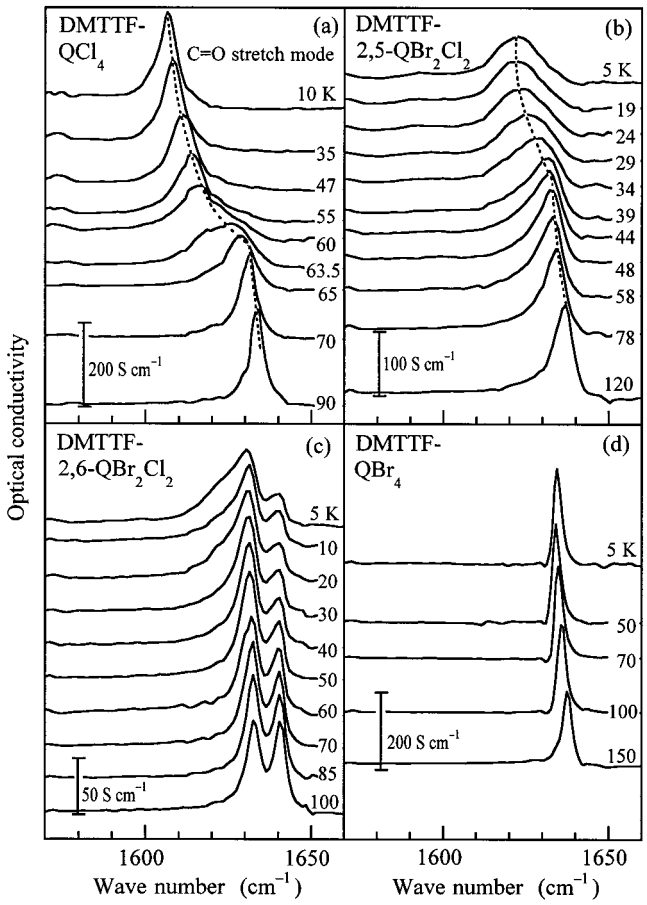

Figure 4. Optical conductivity spectra ($E \perp DA$ stack) for the C═O stretch mode of quinones of (a) DMTTF−QCl_4, (b) DMTTF−2,5-QBr_2Cl_2, (c) DMTTF−2,6-QBr_2Cl_2, and (d) DMTTF−QBr_4 at various temperatures. Dotted lines in parts a and b are guides to the eyes showing the thermal change of peak position in the course of the phase transition.

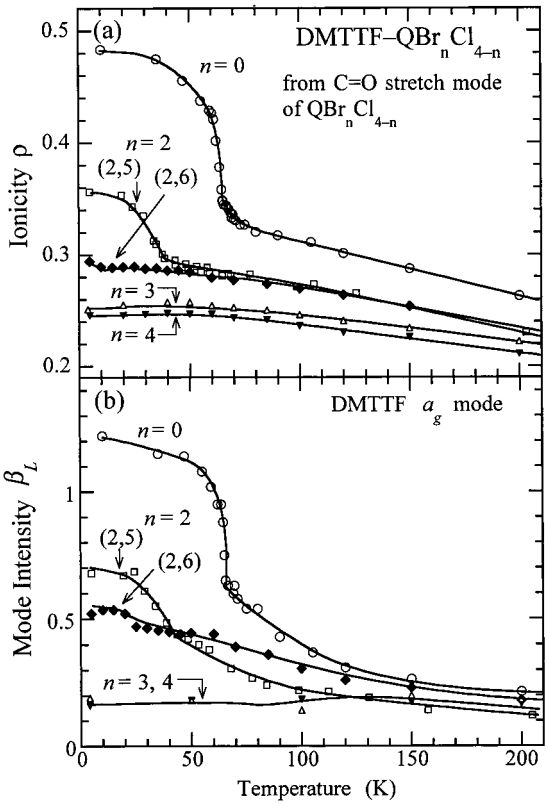

Figure 5. Temperature dependence of infrared molecular vibrational spectra of DMTTF complexes of QCl_4 (open circles), 2,5-QBr_2Cl_2 (open squares), 2,6-QBr_2Cl_2 (filled squares), QBr_3Cl (open triangles), and QBr_4 (filled triangles). (a) Ionicity (ρ) estimated from the frequency $\omega_{C=O}$ of the C═O stretch mode with use of eq 2. (b) Mode intensity β_L of the C═C stretching a_g mode of DMTTF, which represents the local dimeric stack distortion.

complexes investigated here are apparently in the neutral state at room temperature having $\rho \approx 0.2$, which increases gradually with lowering temperature. For the DMTTF−QCl_4 crystal, the transition temperature is characterized as the steep onset in ρ, which varies from nominally "neutral" ($\rho \approx 0.3$) to more "ionic" ($\rho = 0.4-0.5$) with lowering temperature.[19] The ρ value of the 2,5-QBr_2Cl_2 complex displays an analogous kink-like anomaly with steep increase from $\rho = 0.30$ at the critical temperature of the dielectric transition ($T_c = 49$ K), although its increment below T_c becomes modest compared to the case of DMTTF−QCl_4. For the crystals of 2,6-QBr_2Cl_2, QBr_3Cl, and QBr_4, on the other hand, lack of ρ anomalies is apparently related to the absence of dielectric phase transition. The electronic state of the quantum paraelectric 2,6-QBr_2Cl_2 complex seems to be on the verge of the valence transition at the lowest temperature, where the ρ value is increased up to 0.30, the observed critical value for the 2,5-substituted compound at T_c (see and compare the ρ values in Figure 5a). For $n = 3$ and 4, on the other hand, the thermal ρ-variation as well as the ρ value at the lowest temperature is further diminished with increased Br content, indicating the stabilization of the high-temperature neutral phase.

(19) Reference 4 postulated the low-temperature phase of DMTTF−QCl_4 as a neutral−ionic coexisting state: two absorption bands around 1570−1640 cm^{-1} in the powder spectra were tentatively assigned to the C═O stretching bands of distinctly charged quinone molecules. However, the present polarized spectra of a single crystal clearly rule out this possibility: only the higher frequency band is observed, whereas the other should be assigned to the a_g mode activated in the *E*//stack polarization.

Degree of Dimerization. Similar thermal changes are discerned in the degree of local dimerization, which activates the a_g vibration modes in the *E*//stack polarized spectrum via the electron−molecular vibration interaction.[6,20] The intensity of the band is proportional to the squared amplitude of the local distortion.

Before analyzing the temperature-dependent a_g mode intensity, some spectral features are noted here. Figure 6 shows the thermal behavior of the *E*//stack reflectivity spectra of DMTTF−QBr_nCl_{4-n} complexes in the region of 1300−1500 cm^{-1} to depict the most intense band, which is ascribed to the C═C stretching a_g mode of the DMTTF moiety. For a DMTTF−QCl_4 crystal, the band intensity increases on lowering the temperature (Figure 6a) particularly around $T_c = 65$ K, signaling the *DA* dimerization in the course of ferroelectric transition, as in the case of TTF−QCl_4.[6,10] A sharp dip structure at 1376 cm^{-1} on the broad band of the a_g mode at low temperature (Figures 6a−c) is merely the interference effect on the total reflection band due to a superposing weak band of different origin, presumably related to the H−C−H bending vibration of DMTTF methyl groups.[21]

Even in the high-temperature phase without long-range ordering, the a_g band is still discerned, indicating the presence of local and/or dynamic dimeric distortion. The a_g band is split into two bands, which are rapidly separated away with temperature as denoted by A and B in Figure 6. The two bands do

(20) Rice, M. J.; Lipari, N. O.; Strässler, S. *Phys. Rev. Lett.* **1977**, *39*, 1359.

(21) Meneghetti, M.; Bozio, R.; Zanon, I.; Pecile, C.; Ricotta, C.; Zanetti, M. *J. Chem. Phys.* **1984**, *80*, 6210.

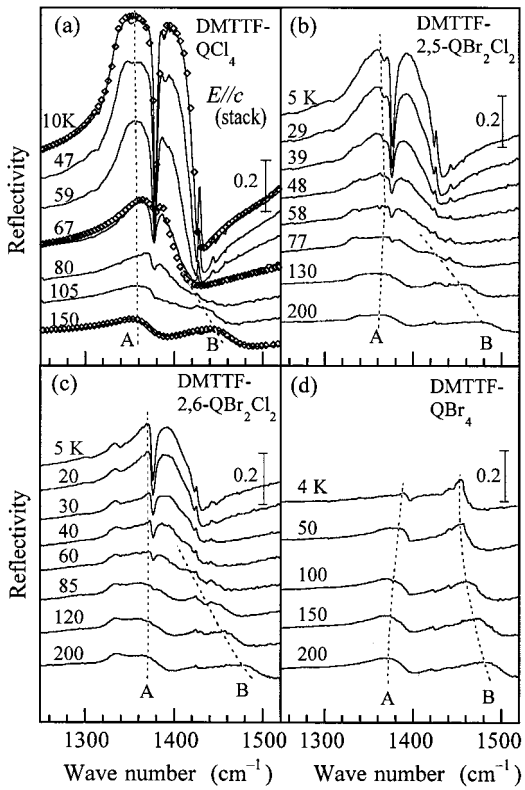

Figure 6. *E*//*c* (*DA* stack) polarized reflectivity spectra showing the C═C stretching a_g mode of DMTTF for (a) DMTTF−QCl_4, (b) DMTTF−2,5-QBr_2Cl_2, (c) DMTTF−2,6-QBr_2Cl_2, and (d) DMTTF−QBr_4 complexes at various temperatures. Dotted curves represent the mode splitting into A and B bands. Small open squares on the 10, 67, and 150 K spectra in part a exemplify the curve fitting with use of the Lorentz oscillator model (eq 3), from which the mode intensity (polarizability) β_L is derived.

not coalesce even at the lowest temperature for the complexes of $n = 3$ and 4 (Figure 6d) with the stable neutral ground state. Such a peculiar mode coalescence/splitting has also been found in the thermal spectral changes for the neutral phase of the typical NI transition system TTF−QCl_4/$QBrCl_3$.[10] The present results for the DMTTF complexes may be interpreted analogously. That is, the split bands arise from the dynamic dimeric distortion with a temporal valence fluctuation: the high-frequency band B is the local dimeric distortion of the host neutral lattice and the low-frequency band A with little frequency change originates from a small portion of the thermally activated ionic region with stronger dimeric distortion.[10] Due to the strong and nonlinear ρ-dependence of the mode frequency particularly for low ρ,[22] the observed large red shift of the B band on cooling is related to the ρ change varying from 0.2 to 0.3. The coalescence of the B band into the A band may arise from the diminished difference in ρ of the two domains and/or from some rapid valence fluctuation mediated by the domain-wall motion.[10] To discuss the total amplitude of dimeric distortion, we employ the sum of the a_g mode intensity for these split bands below.

Figure 5b plots the thermal change of total intensity β_L of the C═C stretching a_g mode as a measure of stack dimerization for various DMTTF−QBr_nCl_{4-n} complexes. The intensity was analyzed by the Lorentz oscillator model, which describes the frequency(ω)-dependent dielectric function,

$$\epsilon(\omega) = \epsilon_\infty + \sum_i 4\pi\omega_i^2\beta_i/(\omega_i^2 - \omega^2 - i\omega\Gamma_i) \qquad (3)$$

Here, ϵ_∞ is the high-frequency dielectric constant, β_i the polarizability (mode intensity), and Γ_i the line width of the i-th band at frequency ω_i. For a DMTTF−QCl_4 crystal, the β_L increases on cooling toward T_c, showing the increasing amplitude of local dimeric distortion. The steep rise of β_L below T_c is due to the development of long-range stack-dimerization. A similar temperature dependence is found for the 2,5-QBr_2Cl_2 complex, although the smaller β_L indicates less magnitude of stack-dimerization below the lowered T_c. For the 2,6-QBr_2Cl_2 complex, the β_L shows more moderate increase without appreciable anomaly of phase transition toward low temperature. At the lowest temperature, the β_L is comparable to that of the 2,5-QBr_2Cl_2 complex at T_c. This observation confirms again the quantum-paraelectric state where the dynamic lattice distortion is enhanced in such a close proximity to the ferroelectric transition. The β_L is rather diminished with flat temperature-dependence for the complexes of QBr_3Cl and QBr_4, in agreement with the released ferroelectric lattice instability.

The ionicity and local dimeric distortion display almost parallel thermal behaviors, as can be seen in Figures 5a and 5b, indicating their strong mutual coupling. The phase transitions of the DMTTF−QBr_nCl_{4-n} system show the features of a continuous (second-order-like) transition in the dielectric susceptibility, ionicity, and local dimeric distortion, in contrast with the typical first-order NI transition in the TTF−QCl_4/$QBrCl_3$ crystals.

Phase Diagram and Quantum Critical Behavior of Ferroelectricity. The ferroelectric valence transition of a series of DMTTF complexes provides a novel phase diagram with quantum critical behavior as described below, although such examples are still rare even among the well-explored ferroelectric perovskite oxides. According to the quantum-theoretical treatment, the transition temperature of ferroelectrics varies as $T_c \propto (S - S_c)^{1/\Phi}$ with $\Phi = 2$ near 0 K, in contrast with $\Phi = 1$ for the classical limit.[23] Here S is the external control parameter such as pressure, chemical composition, or stress[24] and S_c is its value at $T_c = 0$. The ϵ value near $S = S_c$ is predicted to increase as $\epsilon(T \rightarrow 0) \propto (S - S_c)^{-1}$.[23] Figure 7a shows the T_c of DMTTF−QBr_nCl_{4-n} crystals as a function of the lattice parameter c, which can be viewed as the parameter S for the present ferroelectric transition.

In general for the NI transition, the ionic phase is stabilized with the increment of T_c upon applying pressure, because the resultant lattice contraction gains the electrostatic interaction predominantly along the mixed *DA* stack.[1c] For the pressurized DMTTF−QCl_4 crystal, T_c approaches room temperature at about 0.7−1.2 GPa.[4b] Assuming the linear pressure (P)−T_c relationship, the rate of elevating T_c with contraction of the lattice constant c[4b] is evaluated to be 70−110 K per 0.1 Å, using the P-dependent shrinkage of −0.29 Å/GPa.[25] The observed phase boundary (Figure 7a) connecting between $n = 0$ and 1 for DMTTF−QBr_nCl_{4-n} can be well accounted for by this estimated slope. This guarantees the lattice constant c as a good parameter representing effective pressure.

In the phase diagram shown in Figure 7a, however, the drop of T_c with increasing c in the $n = 1-3$ region is obviously much steeper than the linear c-dependence, signaling the quantum

(22) Girlando, A.; Pecile, C.; Brillante, A.; Syassen, K. *Solid State Commun.* **1986**, *57*, 891.

(23) (a) Schneider, T.; Beck, H.; Stoll, E. *Phys. Rev.* **1976**, *B13*, 1123. (b) Höchli, U. T.; Weibel, H. E.; Boatner, L. A. *Phys. Rev. Lett.* **1977**, *39*, 1158.

(24) (a) Samara, G. A. *Phys. Rev. Lett.* **1971**, *27*, 103. (b) Fujii, Y.; Uwe, H.; Sakudo, T. *J. Phys. Soc. Jpn.* **1987**, *56*, 1940.

(25) Nogami, Y. Private communication.

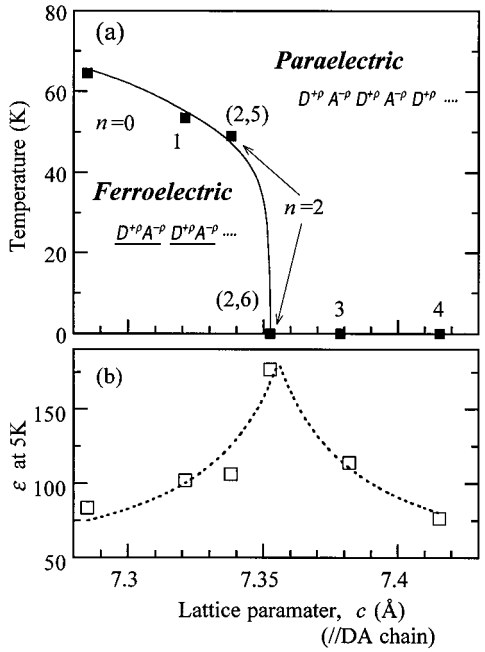

Figure 7. (a) Critical temperature (T_c) and (b) ϵ at 5 K as a function of the lattice parameter c for DMTTF−QBr_nCl_{4-n} crystals. Solid and dotted lines are merely the guide to the eyes.

critical nature. Furthermore, the 2,6-QBr_2Cl_2 complex showing the behavior of quantum paraelectricity stands on the quantum critical point ($T = 0$ boundary) in this phase diagram, at which the low-temperature ϵ value forms a singular peak as the function of S (Figure 7b), as expected. The ionicity and the amplitude of dynamic dimeric fluctuation at the lowest temperature also signify the ground state in the immediate vicinity of the quantum critical point: these values approach the corresponding values of 2,5-QBr_2Cl_2 complex at T_c.

Conclusion

We have systematically investigated the ferroelectric NI phase transition in a series of DMTTF−QBr_nCl_{4-n} complexes. The observed phase boundary can be well described by the lattice expansion by the Br substitution. The present molecular modification can realize a fine-tuning of effective pressure up to −0.2 GPa with varying the Br content n from 0 to 4. Reflecting the close coupling between the ferroelectricity and the valence instability of the molecules, thermal changes of the molecular ionicity and dimerization at T_c are simultaneously diminished with lowering T_c. In particular the 2,6-QBr_2Cl_2 complex has disclosed features of quantum paraelectricity in the vicinity of the quantum ($T = 0$ K) critical point. The observed behaviors near this quantum critical point indicate the novel electronic state of the *DA* complex in which the valence state undergoes the quantum fluctuation, coupled with the dynamical ferroelectric stack-dimerization.

Acknowledgment. We would like to thank N. Nagaosa, T. Luty, G. Saito, and H. Tachibana for enlightening discussions and Y. Nogami for allowing us to present his high-pressure X-ray data. This work, partly supported by NEDO, was performed in the Joint Research Center for Atom Technology (JRCAT) under the joint research agreement between the National Institute for Advanced Interdisciplinary Research (NAIR) and the Angstrom Technology Partnership (ATP).

Supporting Information Available: Tables of atomic coordinates, anisotropic thermal parameters, and bond lengths and angles for DMTTF−QBr_nCl_{4-n} at room temperature (PDF). This material is available free of charge via the Internet at http://pubs.acs.org.

JA0016654